ACS NANO

www.acsnano.org

ARTICLE

Alkali Doping Leads to Charge-Transfer Salt Formation in a Two-Dimensional Metal–Organic Framework

Phil J. Blowey,[#] Billal Sohail,[#] Luke A. Rochford, Timothy Lafosse, David A. Duncan, Paul T. P. Ryan, Daniel Andrew Warr, Tien-Lin Lee, Giovanni Costantini, Reinhard J. Maurer,* and David Phillip Woodruff*

Cite This: *ACS Nano* 2020, 14, 7475–7483

Read Online

ACCESS | Metrics & More | Article Recommendations | Supporting Information

ABSTRACT: **Efficient charge transfer across metal–organic interfaces is a key physical process in modern organic electronics devices, and characterization of the energy level alignment at the interface is crucial to enable a rational device design. We show that the insertion of alkali atoms can significantly change the structure and electronic properties of a metal–organic interface. Coadsorption of tetracyanoquinodimethane (TCNQ) and potassium on a Ag(111) surface leads to the formation of a two-dimensional charge transfer salt, with properties quite different from those of the two-dimensional Ag adatom TCNQ metal–organic framework formed in the absence of K doping. We establish a highly accurate structural model by combination of quantitative X-ray standing wave measurements, scanning tunnelling microscopy, and density-functional theory (DFT) calculations. Full agreement between the experimental data and the computational prediction of the structure is only achieved by inclusion of a charge-transfer-scaled dispersion correction in the DFT, which correctly accounts for the effects of strong charge transfer on the atomic polarizability of potassium. The commensurate surface layer formed by TCNQ and K is dominated by strong charge transfer and ionic bonding and is accompanied by a structural and electronic decoupling from the underlying metal substrate. The consequence is a significant change in energy level alignment and work function compared to TCNQ on Ag(111). Possible implications of charge-transfer salt formation at metal–organic interfaces for organic thin-film devices are discussed.**

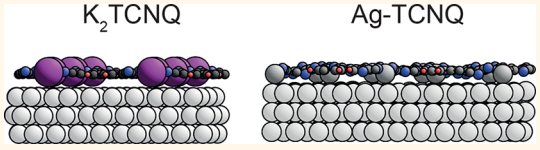

KEYWORDS: *surface structure, charge transfer, two-dimensional salt, X-ray standing waves, density functional theory*

Understanding the interaction between molecules relevant to organic electronics and metallic electrodes is essential due to the critical role that metal–organic interfaces play in determining the electronic properties of the resulting devices. One molecule that has attracted considerable interest as an additive in organic electronics, due to its strong electron acceptor properties, is 7,7,8,8-tetracyanoquinodimethane (TCNQ), and there have been a number of model studies of TCNQ on coinage metal surfaces (*e.g.*, refs 1–8). It has been shown that strong charge transfer between a metal surface and TCNQ modifies the surface work function and provides an important route to control the charge injection barrier between the organic photoactive layer and the conducting electrode in photovoltaic devices and organic light-emitting diodes.[9,10] In this scenario, the surface acts as an electron donor. With the increasing need to achieve further fine-tuning of charge transport across metal–organic junctions, *n*- and *p*-dopants such as alkali salts and metal oxides are often being introduced.[11−13] Hereby, in particular, the interplay between different donor and acceptor species becomes interesting. By including atoms or molecules that are strong donors of electrons into the TCNQ-metal interface, a competition between donor, acceptor, and metal can be created, which has the potential to modify structure, stability, and the ensuing electronic properties of the interface. For example, these ideas have been explored by a density functional theory (DFT) investigation of TCNQ coadsorbed with alkali atoms on a silver surface, which has highlighted the potential to control electrostatic properties such as the surface work function and thus the energy barrier at the metal–organic interface.[14]

Here, we present a comprehensive experimental and theoretical investigation of TCNQ coadsorbed with K on

Received: April 14, 2020
Accepted: May 11, 2020
Published: May 11, 2020

Ag(111) to form a commensurate K_2TCNQ overlayer phase, including a quantitative experimental determination of key structural parameters (using the normal incidence X-ray standing wave—NIXSW—technique[15]) and DFT calculations that take accurate account of both dispersion interactions and charge rearrangement at the interface. We find that, only by correctly describing the effect that the strong charge-transfer between alkali atoms and TCNQ has on the long-range dispersion interactions of the system, can we understand the structure and stability of the interface. Detailed analysis of the electronic structure of the 2D metal−organic-framework (2D-MOF) formed by this coadsorption reveals it to be a *de facto* quasi-free-standing two-dimensional organic salt, formed at the expense of a strongly reduced interaction between the metal surface and the molecular adlayer. This interaction competition between donor, acceptor, and metal directly translates into changes in molecular energy level alignment and work function, both of which can potentially be further tuned by various means. This behavior contrasts with the more typical 2D-MOF formed by TCNQ and Ag adatoms in the absence of the coadsorbed K.

RESULTS AND DISCUSSION

Surface Characterization. Using STM and MCP-LEED two distinct coadsorption phases with good long-range order were identified, one commensurate with the surface unit mesh defined by the matrix $\begin{pmatrix} 3 & 0 \\ 1 & 5 \end{pmatrix}$ and a second incommensurate phase.[16] As realistic simulations using DFT can only be performed for commensurate phases, we present here only the results for this phase, for which STM images and a LEED pattern are shown in Figure 1.

In at least some studies of atom/molecule coadsorption phases, STM images show features that can be assigned to the location of the coadsorbed metal atoms (*e.g.*, refs 17 and 18); in these cases, the STM images can be used to determine the relative numbers of adsorbed metal atoms and molecules. Evidently this is not the case in the images shown in Figure 1. In Figure 1b, in particular, the only visible features have a shape and size that is consistent with individual TCNQ molecules, with no intermediate atomic protrusions. The superimposed structural model in a single unit mesh does show, in red, the location of K atoms indicated by the DFT-optimized structural model discussed below, but there are no corresponding features in the experimental image. This apparent "STM-invisibility" of metal adatoms in such structures is not rare, and also occurs in the case of the commensurate phase of TCNQ alone on Ag(111),[8] as well as in other systems (*e.g.*, ref 19); it reflects the fact that STM is a probe of the electronic surface above the surface, not the atomic locations within it. A simulated image of this surface, derived from our DFT calculations using the standard Tersoff−Hamman[20] approach (Figure S2), also fails to show any features due to the presence of the K atoms. Indeed, a STM investigation of coadsorption of K with PTCDA on this surface also obtained images in which the K atoms were "invisible", although in this study much higher resolution images, acquired at much smaller tip−surface separation by using scanning tunnelling hydrogen microscopy (STHM), did locate the K atoms.[21] The alternative and more widely applicable (and intrinsically quantitative) route to determining the stoichiometry used here is from the XPS peak intensities,

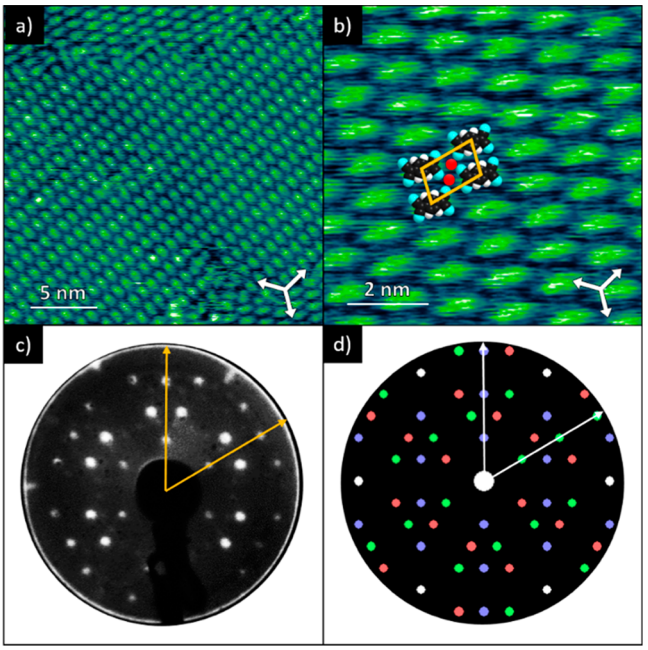

Figure 1. (a, b) Constant current STM images (−0.6 V, 100 pA) of the commensurate coadsorption phase of K and TCNQ on Ag(111) at two different magnifications. (c) MCP-LEED pattern from this surface at an electron energy of 24.5 eV. (d) Simulation of this pattern using LEEDpat;[22] different colors correspond to different rotational and mirror domains. Superimposed on (b) is the unit mesh and a structural model. The arrows show the ⟨110⟩ close-packed azimuthal directions on the surface.

corrected for photon energy dependent photoionization cross sections.

Figure 2 shows high-resolution SXP spectra recorded at a photon energy of 435 eV for the C 1s and K 2p peaks and at a

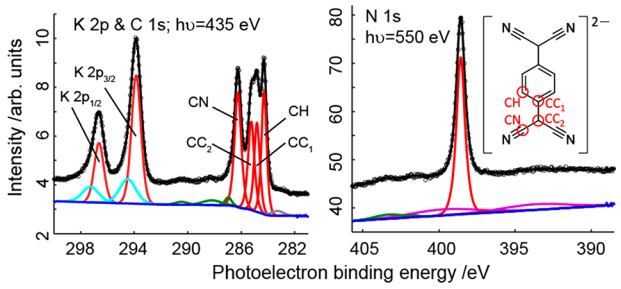

Figure 2. High-resolution SXP spectra from K/TCNQ coadsorption in the commensurate ordered phase on Ag(111). The fits (black lines) to the raw spectra (individual experimental points) comprise several components indicated by the colored lines. The main components of the C 1s, K 2p and N 1s are all shown in red. The minor K 2p component is shown in cyan. In addition are shown shake up features (green), a very small C 1s beam damage component (gray), a Shirley background to the K 2p/C 1s spectrum (blue) and a linear background to the N 1s spectrum (blue).

photon energy of 550 eV for the N 1s peak. The K 2p spectra show two chemically shifted spin−orbit split components, the main components (red) and smaller second components (cyan). This second component is attributed to excess K atoms not accommodated in the ordered single-layer coadsorption structure. Comparison of the intensities of the main K 2p

https://dx.doi.org/10.1021/acsnano.0c03133
ACS Nano 2020, 14, 7475−7483

component and C and N 1s peaks in our SXP spectra indicates an approximate K:TCNQ stoichiometry of 2.4:1, which with typical precision estimates of ∼ ± 20% for this measurement, would be consistent with a K_2TCNQ layer; this is the basis of the structural model identified by the DFT calculations and shown schematically superimposed in Figure 1b. The chemically shifted component of the K 2p peaks (cyan) indicates an approximate 30% excess relative to that accommodated in the ideal K_2TCNQ stoichiometry.

The N 1s spectrum shows a single sharp peak consistent with an intact adsorbed TCNQ molecule; the background under this peak contains weak features due to a shakeup satellite (green) and to plasmon losses on the Ag 3d emission (purple line). The C 1s spectrum contains four chemically shifted components assigned to the different C bonding environments as indicated in the figure. The C 1s XP spectrum for the commensurate phase of pure TCNQ on Ag(111) has previously been noted to be consistent with the expected electron transfer from the substrate to the molecule.[8] However, in the presence of the coadsorbed K there are further small decreases in the photoelectron binding energies (see Table S1) consistent with additional accumulation of negative charge on the molecule, as might be expected from the presence of the strong electron donor characteristics of the coadsorbed K.

Work function measurements previously reported[23] yielded values for the clean Ag(111) surface of 4.59 ± 0.05 eV and for the commensurate phase of pure TCNQ on Ag(111) of 5.02 ± 0.05 eV. The K_2TCNQ overlayer phase was found to have a work function of 3.92 ± 0.05 eV. These measurements were made by recording the secondary electron cutoff of ultraviolet photoemission spectra (UPS) with an applied bias of −10 V to the sample (see Figure S2a). The corresponding changes in work function relative to the clean surface are thus +0.43 eV after TCNQ deposition and −0.67 eV with the K_2TCNQ overlayer. These compare with values derived from the DFT calculations (see the Supporting Information) of +0.47 and −0.31 eV, respectively. The larger reduction seen in the experiment relative to the calculated value for the K_2TCNQ phase may be partly attributed to the presence of the excess K discussed previously.

Structure and Bonding: NIXSW and DFT Results. The NIXSW technique allows one to extract the height above the surface of each locally inequivalent atom in the overlayer in an element- and chemical-state-specific manner.[15] Measured NIXSW absorption profiles can be fitted by just two structural parameters, the coherent fraction, *f*, and the coherent position, *p*. The coherent fraction is commonly regarded as an order parameter, and values of ∼0.8 generally indicate that the coherent position corresponds to the height of the absorbing atoms relative to the atomic scattering planes of the Bragg reflection. However, much lower values of *f* indicate that there are likely to be two or more contributing heights, the measured coherent position being some weighted average of these different values. The coherent position *p* can be converted to a height using the conversion formula $D = (n + 1)d_{(111)}$, where $d_{(111)}$ is the Ag(111) bulk interlayer spacing and *n* is an integer, chosen to ensure that interatomic bond lengths between the substrate and the molecule fall in a physically reasonable range.[15]

NIXSW measurements using the (111) Bragg reflection were acquired from multiple preparations of the K_2TCNQ surface phase, using SXPS recorded before and after these measurements to confirm that there was no evidence of radiation damage. The resulting photoemission-monitored absorption profiles are shown in Figure S1. Table 1 summarizes the atomic height parameters extracted from these NIXSW measurements from the K_2TCNQ overlayer and compares them with the values previously reported[8] for the TCNQ overlayer in the commensurate phase which comprises a 2D-MOF of Ag adatoms and TCNQ. The associated coherent fraction values are reported in Table S2 and discussed in detail in the Supporting Information.

Table 1. Comparison of the Coherent Position Values, Converted into Heights, Extracted from the NIXSW Measurements for the Commensurate Overlayer of Ag−TCNQ on Ag(111)[8] and the Commensurate Coadsorption Phase K_2TCNQ on Ag(111)[a]

	D (Å)	
component	Ag−TCNQ	K_2TCNQ
CH	2.86(5)	2.97(5)
CC	2.78(5)	2.99(5)
CN	2.76(5)	3.22(5)
N	2.75(5)	3.30(5)
K (main)		3.29(7)
K (minor)		3.65(16)

[a]Precision estimates, in units of 0.01 Å, are shown in parentheses.

To understand the full structural and bonding implications of these results, dispersion-inclusive DFT calculations using the PBE+vdW^{surf} and PBE+MBD functionals were undertaken. As will be shown below, these calculations provide details of a structural model that proves not only to be consistent with the NIXSW results but also gives insight into the nature of the bonding within the 2D-MOF and to the underlying substrate and identifies the thermodynamic driving force behind 2D-MOF formation. Calculations were performed using the $\begin{pmatrix} 3 & 0 \\ 1 & 5 \end{pmatrix}$ unit mesh found in the experiments, containing two K atoms and a TCNQ molecule, as guided by the experimentally inferred composition ratio.

Figure 3 depicts the optimized structure as predicted by the PBE+vdW^{surf} method, which comprises alternating K and TCNQ stripes oriented along the ⟨110⟩ directions of the surface. A range of alternative structural models, reflecting alternative locations of the K atoms relative to the TCNQ molecules, were explored to identify the lowest energy structure. The K atoms appear to be 4-fold coordinated by the cyano groups of neighboring TCNQ molecules. In addition, parts c and d of Figure 3 show the TCNQ overlayer phase prior to K deposition, which has been previously identified by a joint NIXSW and DFT study.[8] This phase, which we hereafter refer to as Ag−TCNQ, features Ag adatoms and TCNQ molecules in a ratio of 1:1, although there is some evidence that the three Ag adatom sites per unit mesh may not all be 100% occupied.[8] Note that this structure was previously calculated with PBE+D3[24] but is reoptimized here with PBE+vdW^{surf}. The minor differences in lateral registry between the results of these two calculations do not significantly alter the agreement with NIXSW structural data. The adsorption heights predicted by the standard versions of two dispersion-inclusive DFT methods for the K_2TCNQ overlayer (see Table 2) are systematically lower than the experimentally measured XSW results. This underestimation is stronger for the K atoms than for the C and N atoms in

https://dx.doi.org/10.1021/acsnano.0c03133
ACS Nano 2020, 14, 7475−7483

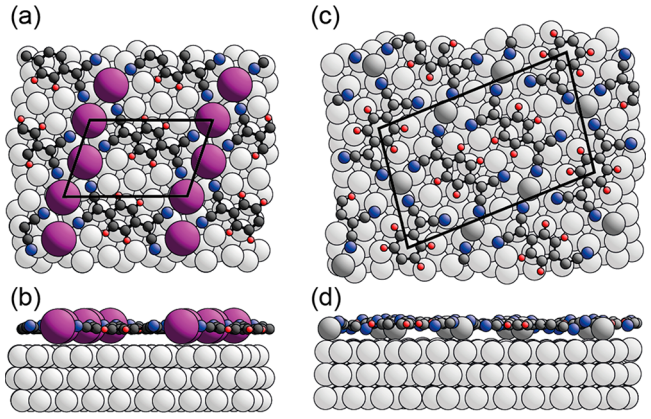

Figure 3. (a) Top view and (b) side view of K_2TCNQ adsorbed on Ag(111) surface. Black lines depict the surface unit mesh. (c) Top view and (d) side view of the previously identified TCNQ overlayer which includes Ag adatoms.[8] The large K atoms are shown in purple; the molecular atoms are C (dark gray), N (blue), and H (red). Ag atoms in the bulk are light gray; Ag adatoms are represented by spheres of the same size but with a darker shade.

Table 2. Comparison of Adsorption Heights (D) of the Spectroscopically Distinct atoms in K_2TCNQ on Ag(111) Overlayers As Measured Experimentally by NIXSW, with Values Predicted by Standard PBE+MBD and PBE+vdW^{surf} Calculations, and by the Same Methods with Rescaled Dispersion Coefficients for Potassium to Account for Strong Charge Transfer (K^+)

	D (Å)				
	CH	CC	CN	N	K
experiment	2.97	2.99	3.22	3.3	3.29
vdW^{Surf}	2.90	2.99	3.17	3.26	2.85
MBD	2.94	3.02	3.16	3.23	2.81
vdW^{Surf}(K^+)	2.93	3.00	3.18	3.32	3.27
MBD(K^+)	2.87	2.98	3.26	3.47	3.17

TCNQ, with both MBD and vdW^{surf} underestimating the K adsorption height by almost 0.5 Å.

This large deviation from experiment in the predicted adsorption height of K could originate from the fact that both PBE+MBD and PBE+vdW^{surf} fail to take sufficient account of the change in atomic polarizability due to strong charge transfer.[25,26] Both methods use the atoms-in-molecules Hirshfeld charge partitioning scheme to adapt the atomic polarizability of individual atoms to their respective chemical environment[27,28] in a molecule or solid. Hirshfeld charge analysis is prone to underestimate charge transfer in polar and ionic situations.[28] In the case of K_2TCNQ, K atoms within the arrangement are predicted by this method to have a net positive charge of 0.30 e (see Table S2).

The iterative Hirshfeld method, which correctly accounts for the effect of strong charge transfer in the partitioning of the electron density,[29] significantly increases this predicted charge transfer to a positive charge of 1.06 e per K atom and a negative charge of −0.70 e per N atom in TCNQ (see Tables S4 and S6 for details). This suggests that upon formation of the coadsorption layer both K and TCNQ are strongly charged (the TCNQ net charge predicted by the iterative Hirshfeld method amounts to −2.03 e corresponding to a fully occupied LUMO orbital), effectively transforming the 2D-MOF into a 2D organic−alkali charge-transfer salt layer. Somewhat similar behavior has been previously observed for coadsorption of K and PTCDA molecules on Ag(111). In this case, very significant differences were also found between the measured and DFT predicted heights of the overlayer, with the discrepancy for the K atoms being 0.49 Å.[30] This is similar to the discrepancies seen in our results using the standard vdW^{surf} and MBD methods. However, inspired by recent work of Bučko and Gould to improve the MBD method to account for strong charge transfer in intermolecular interactions,[25] and encouraged by the benchmark structural information from the NIXSW experiments, we have made a small but important modification to our calculations (see the Supporting Information for further details). We replaced the atomic reference polarizability and C_6 coefficients for neutral K that enter the MBD and vdW^{surf} methods with the respective reference values for K^+ published by Gould and Bučko.[43] On this basis, we reoptimized the K_2TCNQ structure on Ag(111). The results are shown in Table 2 as vdW^{surf}(K^+) and MBD(K^+).

The rescaled coefficients for K yield an overall increase of adsorption height for the molecule and the potassium atoms. For PBE+vdW^{surf}, the adsorption heights for the atomic species in the TCNQ molecule are now in very good agreement (to within 0.04 Å) with experiment. The adsorption heights of K found by vdW^{surf}(K^+) and MBD(K^+) are 3.27 and 3.17 Å, respectively, compared with the experimental value of 3.29 Å. PBE+vdW^{surf} is known to provide excellent structural predictions of metal−organic interfaces,[31,32] although it tends to overestimate adsorption energies. The latter is remedied with the MBD method, but the performance of this method on structural properties is yet to be assessed systematically; it slightly underestimates the adsorption height in the present system. We note that this may be partially due to the strong overestimation of the surface layer relaxation with PBE+MBD for K_2TCNQ. Within the experimental and computational precision estimates, the structural model derived from the PBE +vdW^{surf}(K^+) calculations gives an excellent account of the NIXSW coherent positions. In our further analysis of the driving forces behind K_2TCNQ overlayer formation and the electronic properties of the interface, we will focus on the PBE +vdW^{surf}(K^+) results, which clearly give the best description of the geometry.

Analysis of the Character of the 2D-MOFs: Ag−TCNQ *vs* K_2-TCNQ. Having arrived at an accurate structural model for the 2D-MOF phase K_2TCNQ, we need to understand the driving force for its formation. The structural model for TCNQ on Ag(111) coadsorbed with Ag adatoms (Ag−TCNQ, as shown in Figure 3c,d) is a 2D-MOF of Ag adatoms and TCNQ comprising stripes of TCNQ and stripes of Ag adatoms. Upon exposure to potassium, the Ag adatoms are replaced by K and the structure converts to the K_2TCNQ overlayer phase shown in Figure 3a,b. This transition can occur at room temperature for sufficiently high K coverages but occurs over a wider range of K coverages at slightly elevated temperature, clearly indicating that the replacement of the Ag adatoms with K is energetically favored. A detailed investigation of this transformation using low energy electron microscopy is reported by Haags et al.[23]

We have analyzed the interaction energies of the two overlayer phases on Ag(111), Ag−TCNQ and K_2TCNQ, to assess the interaction competition between the donor (K), acceptor (TCNQ), and the metal surface; these are shown in Figure 4. The left-hand column of Figure 4 reports the total

https://dx.doi.org/10.1021/acsnano.0c03133
ACS Nano 2020, 14, 7475−7483

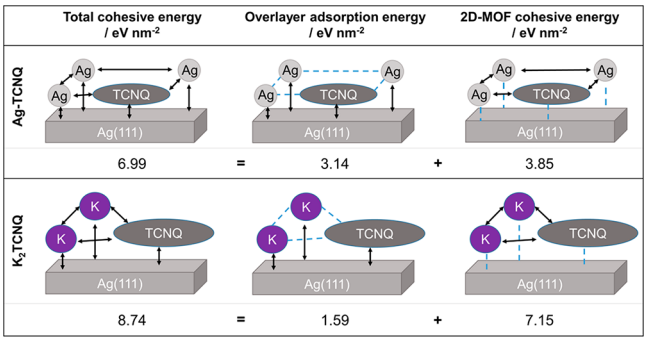

Figure 4. Schematic depictions of the energetic contributions to the adsorption energy of the two overlayer structures on Ag(111): Ag−TCNQ (top row) and K_2TCNQ (bottom row). The left column shows the total adsorption energy of the overlayer at the metal surface per unit surface area (nm^2). The center column identifies the interaction energy of the overlayer components and the metal surface. The right column shows the cohesive energy within the overlayer. Bold arrows denote interactions included in the energies given below; dashed lines indicate interactions that are not included.

cohesive energy, E_c, per unit surface area of the two metal-adsorbed overlayers, which was calculated using eq 1

$$E_c = \frac{[E_{tot} - (E_{2D\text{-}MOF} + E_{surf})]}{E_{ads}} + \frac{[E_{2D\text{-}MOF} - (E_{Ag,K} + E_{TCNQ})]}{E_c^{2D-MOF}} \quad (1)$$

where E_{tot} is the energy of the total system, E_{surf} is the energy of the bare Ag(111) substrate, $E_{2D\text{-}MOF}$ is the energy of the free-standing overlayer of K_2TCNQ or Ag−TCNQ, and E_{TCNQ} is the energy of isolated TCNQ. For the Ag−TCNQ system, the total cohesive energy was calculated with reference to the bulk cohesive energy of Ag−referred to as E_{Ag} in eq 1. Conversely, the K_2TCNQ system used a free K atom as a reference−referred to as E_K in eq 1. E_K was chosen because the SAES dispenser sources, used in the experiments reported here, are known to emit a flux of neutral alkali atoms[33] and that the K_2TCNQ phase forms spontaneously upon K atom adsorption.[23] We find that K_2TCNQ is clearly more stable (8.74 eV nm^{-2}) than Ag−TCNQ (6.99 eV nm^{-2}). As shown in eq 1, we can break down this interaction into the contribution from within the overlayer ($E_c^{2D\text{-}MOF}$, 2D-MOF cohesive energy) and the contribution from the interaction with the substrate (E_{ads}, overlayer adsorption energy). By doing so, we find that, in the case of Ag−TCNQ, these two contributions are similar, *i.e.*, Ag−TCNQ is approximately equally stabilized by the interactions within the overlayer (55%) and the interactions with the substrate (45%). In contrast, in the case of K_2TCNQ, the cohesive energy within the 2D-MOF is substantially larger than the bonding energy to the substrate and constitutes about 82% of the total interaction energy between molecule, adatoms, and substrate. This increase in the strength of the interactions within the layer comes at the expense of overlayer−metal interaction strength, which is reduced from 3.14 to 1.59 eV nm^{-2} when replacing Ag with K adatoms. This is consistent with the larger average molecular adsorption height that is measured by NIXSW and reflected in the calculated structures (see Table 2).

The picture presented by the interaction strength is in line with strong charge transfer within the overlayer, which leads to the formation of a 2D organic salt. Iterative Hirshfeld analysis confirms a net charge of +1.06 *e* on K and a net charge of −2.03 *e* on TCNQ. The net charge transfer between the overlayer and the metal is thus only 0.09 *e* per unit mesh (or 0.08 *e* per nm^2) with electron flow *to* the metal. By contrast, in the case of the Ag−TCNQ overlayer, the overlayer has a net negative charge of −0.85 *e* per nm^2 transferred from the metal substrate. This charge redistribution at the interface is also reflected in the density difference plots shown in Figures S4 and S5.

We can therefore conclude that, upon alkali coadsorption, a structurally and energetically decoupled 2D charge-transfer organic salt layer is formed at the expense of the molecule−metal surface interaction. The structural decoupling is evidenced by the increase in adsorption height of the whole overlayer. The energetic decoupling is evidenced by the decrease of interaction between overlayer and substrate. A similar decoupling effect has been reported previously for alkali coadsorption of PTCDA on Ag(111),[30] albeit using a computational theory (without rescaled coefficients for K^+) that gives inferior agreement with the experimentally measured adsorption heights. The structural and energetic decoupling of the overlayer also has consequences for the energy level alignment at the interface. Figure 5 depicts the average

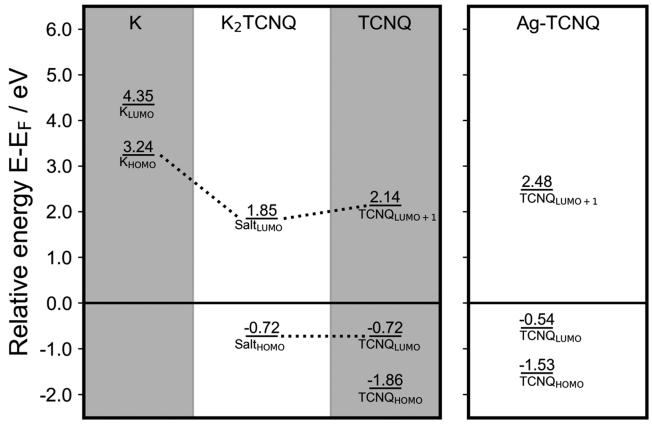

Figure 5. (Left) Ag(111)−K_2TCNQ molecular energy level diagram showing energy levels of K atoms, TCNQ molecules, and of the joint K_2TCNQ salt layer. (Right) Ag(111)-(Ag−TCNQ) molecular energy level diagram showing energy levels of TCNQ molecules. These energy levels are extracted via a molecular orbital projected DOS calculation. Further details are provided in the Supporting Information.

energies of the molecular orbitals projected from the density of states (DOS) of the two interfaces, which are shown in Figure 6 (see the Supporting Information for more details). In the case of Ag−TCNQ, the HOMO and LUMO of the TCNQ molecule, both occupied upon adsorption to the surface, can be found closer to the Fermi level than in the case of K_2TCNQ. In contrast, the LUMO+1 of TCNQ is found higher above the Fermi level for Ag−TCNQ than for K_2TCNQ. A possible reason behind this effect is the difference in adsorption heights between Ag−TCNQ and K_2TCNQ, which leads to a change in orbital renormalization due to the image charge in the substrate.[34] Dotted lines in Figure 5 identify the hybridization contribution of K atom states and

https://dx.doi.org/10.1021/acsnano.0c03133
ACS Nano 2020, 14, 7475−7483

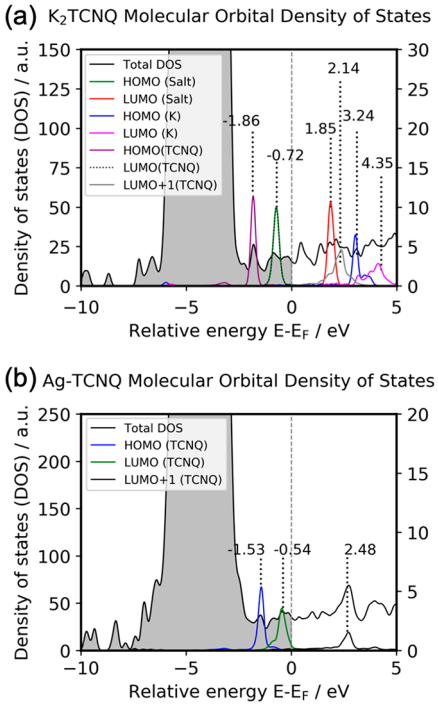

Figure 6. Molecular orbital projected density of states for (a) K_2TCNQ and (b) Ag−TCNQ. Potassium and frontier molecular orbital states (ordinate scale on the right-hand side) have been scaled with respect to the total density of state (ordinate scale on the left-hand side). .

TCNQ molecular states in the formation of the HOMO and LUMO states of the K_2TCNQ salt overlayer. The HOMO of the K_2TCNQ overlayer is almost purely formed by the LUMO of TCNQ, which suggests a mostly electrostatic interaction between K and TCNQ with little covalent interaction. The K_2TCNQ LUMO shows some contribution from the LUMO +1 of TCNQ and the HOMO of the K atoms, which suggests a moderate amount of hybridization in this conduction state. This analysis supports our classification of the K_2TCNQ 2D-MOF as an organic salt. By contrast, Ag−TCNQ shows more complex hybridization between Ag adatoms and TCNQ states, which is also reflected in stronger broadening of molecular energy levels (see Figure 6). In summary, the level alignment of K_2TCNQ corresponds to a reduction of the energy required to generate negative charge carriers (electrons) in the adlayer and an increase in the energy required to generate positive charge carriers (holes) when compared to Ag−TCNQ. The changed level alignment and hybridization of overlayer states with respect to the substrate are evidence for the electronic changes which follow from the structural decoupling due to alkali doping.

The energy level shifts predicted by DFT, from Ag−TCNQ to K_2TCNQ, of the two most shallowly bound orbitals to greater binding energies is reproduced qualitatively by the UP spectra shown in Figure S2(b). We stress that no quantitative agreement between semilocal DFT and UPS is to be expected, as the calculated values are ground state energies, whereas UPS measures excitations due to electron removal.

CONCLUSIONS

Based on detailed experimental characterization using STM, LEED, and SXPS, together with quantitative experimental structural data from NIXSW and dispersion-corrected DFT calculations, we show that the addition of K atoms to the structure formed by TCNQ on Ag(111) leads to profound changes in the structure of the surface layer. Specifically, the K atoms incorporate into a commensurate 2D-MOF phase formed by K and TCNQ that replaces the 2D-MOF formed by TCNQ and Ag adatoms, the molecules being raised significantly higher above the Ag(111) surface. Analysis of the charge transfer and bonding energetics shows that the K/TCNQ layer is actually a 2D charge transfer salt with a high cohesive energy, while both the bonding to, and charge transfer from the substrate are very significantly reduced.

An earlier study of the coadsorption of PTCDA and K on Ag(111) led to somewhat similar conclusions, but with some important differences. Two different coadsorption phases (K_2PTCDA and K_4PTCDA) were identified by LEED, STM, and STHM (scanning tunnelling hydrogen microscopy)[21] to be incommensurate with the substrate, and so, in order to model these with DFT calculations, the underlying Ag(111) substrate was artificially strained to allow the overlayer to be commensurate. Subsequently,[30] the results of NIXSW experiments from the K_2PTCDA phase were reported, providing reliable measurements of the heights above the surface of the constituent atoms of the overlayer. However, the DFT calculations of the detailed structure yielded values of the heights of the overlayer atoms in rather poor agreement with the experimental values; the molecular atom heights differed by 0.18−0.27 Å while for the K atoms the discrepancy was 0.49 Å. This later paper[30] also presented the results of differential reflectance spectroscopy measurements, the interpretation of which was stated to be ambiguous but nevertheless claimed to support the decoupling of the PTCDA overlayer following K deposition. By contrast, we present a comprehensive investigation of a *commensurate* 2D-MOF phase formed by K and TCNQ, and by Ag adatoms and TCNQ, on Ag(111). Only by fully accounting for the charge state of the potassium atoms in the K_2TCNQ coadsorption phase, we arrive at a dispersion-inclusive DFT description of this quasi-free-standing 2D-MOF which is in excellent agreement with experimental NIXSW measurements. We find that the charge-transfer-driven donor−acceptor K−TCNQ interaction is very strong, effectively reducing the TCNQ−metal and K−metal interaction when compared to pure K/metal and TCNQ/metal adsorption heights. As described in detail above, the formation of a 2D organic K−TCNQ salt layer with a high cohesive energy leads to decoupling from the metal surface when compared to Ag−TCNQ. This decoupling is evidenced by changes in the structure, the energy level alignment and hybridization, the work function at the interface with the organic alkali salt, and the charge injection barriers relative to that of the pure TCNQ overlayer. Alkali doping of organic semiconductors is common (*e.g.*[35]) and a decoupling effect due to alkali doping at metal interfaces has been proposed before. However, here we have been able to fully rationalize this phenomenon, which has only been possible by including the effects of a strong charge-transfer on the long-range dispersion interactions of the system. In fact, our detailed analysis demonstrates that only by correctly describing this effect it becomes possible to fully account for the structural and electronic properties of this kind of 2D charge transfer salts.

The significant effect of alkali doping and charge-transfer salt formation on measurable electronic properties suggests that a certain level of control could be exerted over these properties

https://dx.doi.org/10.1021/acsnano.0c03133
ACS Nano 2020, 14, 7475−7483

by varying the structure and composition of such charge-transfer salts. This could include variation of the strength of the donor and acceptor components, as well as their occupation ratio and the reactivity of the underlying substrate. The decoupling of the 2D-MOF salt from the metal surface also raises interesting questions as to whether this effect is widespread in alkali-doped organic electronics and whether it is beneficial or harmful for practical devices.

METHODS

Initial characterization of the Ag(111) surface was conducted at the University of Warwick in an ultrahigh vacuum (UHV) chamber equipped with a scanning tunneling microscope (STM) and a low energy electron diffraction optics fitted with microchannel plate amplification (MCP-LEED) to allow operation at low incident beam currents. Synchrotron radiation X-ray photoelectron spectroscopy (SXPS) characterization and normal incidence X-ray standing wave (NIXSW) measurements were performed in the UHV end-station installed on beamline I09 of the Diamond Light Source.[36] MCP-LEED at both locations provided a valuable cross-reference for the preparation of equivalent adsorbed layers. The single crystal Ag(111) sample was cleaned *in situ* using cycles of 1 keV Ar^+ ion bombardment and by annealing.

NIXSW measurements to monitor the X-ray absorption at the C and N atoms of TCNQ, as well as at the coadsorbed K atoms, were achieved by measuring the intensity of the C 1s, N 1s, and K 2p photoelectron spectra, collected to allow chemical-state specific NIXSW data to be extracted. Fitting of the NIXSW absorption profiles to extract the structural parameters included taking account of the nondipolar effects on the angular dependence of the photoemission, using values for the backward-forward asymmetry parameter Q,[37] obtained from theoretical angular distribution parameters.[38] Work functions were determined by measuring the secondary electron cutoff in ultraviolet photoelectron spectroscopy (UPS) using a standard He I source ($h\nu$ = 21.23 eV) with a bias of −10.00 V applied to the sample; similar UPS facilities were used in both the Warwick and Diamond chambers.

The K/TCNQ networks were prepared *in situ* by first depositing a nominally saturated single layer of TCNQ onto Ag(111), followed by annealing to 280 °C to yield the commensurate $\begin{pmatrix} 2 & 5 \\ -8 & -2 \end{pmatrix}$ submonolayer adsorption phase after cooling.[8] K was then deposited from a SAES dispenser source onto the sample, which was then annealed to 200 °C to promote the formation of ordered TCNQ/K coadsorption networks as judged by LEED.

DFT calculations were performed with the FHI-aims package,[39] and a GGA-PBE functional[40] was used to evaluate exchange-correlation. Dispersion interactions were modeled using both the Tkatchenko−Scheffler vdW^{surf} method (DFT+vdW^{surf})[41] and the many-body dispersion method (DFT-MBD)[42,43] implemented in the FHI-aims package. The original DFT+vdW^{surf} C_6 and polarizability coefficients[40] (used in both the DFT+vdW^{surf} [40] and DFT-MBD[41,42] dispersion corrections) were modified for K, using values proposed by Gould and Bucko,[44] to account for the ionic nature of the alkali atoms within the donor−acceptor networks formed with TCNQ. The adsorption structure was modeled as a periodically repeated cell comprising a single unit mesh of the commensurate K_2TCNQ adsorption phase on Ag(111) described by a $\begin{pmatrix} 3 & 0 \\ 1 & 5 \end{pmatrix}$ matrix of the substrate lattice vectors, containing a single TCNQ molecule and two K atoms. The Ag(111) surface was modeled as a slab consisting of four atomic layers and separated from its periodic image by a vacuum gap exceeding 35 Å. The coordinates of the atoms in the bottom two layers of the Ag slab were constrained to the bulk truncated structure of Ag and the positions of all other atoms in the simulation cell were relaxed. The Brillouin zone was sampled with a 4 × 4 × 1 Monkhorst−Pack[45] k-grid, and the geometries were optimized to below a force threshold of 0.025 eV $Å^{-1}$. Further method details including some additional references[46−48] can be found in the Supporting Information. All calculation inputs and outputs have been deposited as a data set in the NOMAD repository (https://repository.nomad-coe.eu/) and are freely available.[49]

ASSOCIATED CONTENT

Supporting Information

The Supporting Information is available free of charge at https://pubs.acs.org/doi/10.1021/acsnano.0c03133.

NIXSW data analysis and STM image simulations; computational details of DFT calculations; details of dispersion parameter rescaling for potassium; charge analysis for K_2-TCNQ and Ag−TCNQ on Ag(111); calculation of energy level diagrams of K_2-TCNQ and Ag−TCNQ on Ag(111); calculation of work function of K_2-TCNQ and Ag−TCNQ on Ag(111); density difference plots of K_2-TCNQ and Ag−TCNQ on Ag(111) (PDF)

AUTHOR INFORMATION

Corresponding Authors

Reinhard J. Maurer − *Department of Chemistry, University of Warwick, Coventry CV4 7AL, U.K.*; orcid.org/0000-0002-3004-785X; Email: r.maurer@warwick.ac.uk

David Phillip Woodruff − *Department of Physics, University of Warwick, Coventry CV4 7AL, U.K.*; orcid.org/0000-0001-8541-9721; Email: d.p.woodruff@warwick.ac.uk

Authors

Phil J. Blowey − *Department of Physics and Department of Chemistry, University of Warwick, Coventry CV4 7AL, U.K.*

Billal Sohail − *Department of Chemistry, University of Warwick, Coventry CV4 7AL, U.K.*

Luke A. Rochford − *Chemistry Department, University of Birmingham, Birmingham B15 2TT, U.K.*

Timothy Lafosse − *Department of Chemistry, University of Warwick, Coventry CV4 7AL, U.K.*

David A. Duncan − *Diamond Light Source, Harwell Science and Innovation Campus, Didcot OX11 0DE, U.K.*; orcid.org/0000-0002-0827-2022

Paul T. P. Ryan − *Diamond Light Source, Harwell Science and Innovation Campus, Didcot OX11 0DE, U.K.; Department of Materials, Imperial College, London SW7 2AZ, U.K.*

Daniel Andrew Warr − *Department of Chemistry, University of Warwick, Coventry CV4 7AL, U.K.*

Tien-Lin Lee − *Diamond Light Source, Harwell Science and Innovation Campus, Didcot OX11 0DE, U.K.*

Giovanni Costantini − *Department of Chemistry, University of Warwick, Coventry CV4 7AL, U.K.*; orcid.org/0000-0001-7916-3440

Complete contact information is available at: https://pubs.acs.org/10.1021/acsnano.0c03133

Author Contributions

[#]P.J.B. and S.B. contributed equally.

Notes

The authors declare no competing financial interest.

ACKNOWLEDGMENTS

The authors thank Diamond Light Source for allocations SI15899 and NT18191 of beam time at beamline I09 that contributed to the results presented here. P.J.B. acknowledges financial support from Diamond Light Source and EPSRC.

G.C. acknowledges financial support from the EU through the ERC Grant "VISUAL-MS" (Project ID: 308115). B.S. and R.J.M. acknowledge doctoral studentship funding from the EPSRC and the National Productivity Investment Fund (NPIF). R.J.M. acknowledges financial support via a UKRI Future Leaders Fellowship (MR/S016023/1). We acknowledge computing resources provided by the EPSRC-funded HPC Midlands+ Computing Centre (MR/S016023/1) and the EPSRC-funded Materials Chemistry Consortium for the ARCHER U.K. National Supercomputing Service (EP/R029431/1). R.J.M. acknowledges fruitful discussions with O. Hofmann (TU Graz).

REFERENCES

(1) Stradi, D.; Borca, B.; Barja, S.; Garnica, M.; Diaz, C.; Rodriguez-Garcia, J. M.; Alcami, M.; Vazquez de Parga, A. L.; Miranda, R.; Martin, F. Understanding the Self-Assembly of TCNQ on Cu(111): a Combined Study Based on Scanning Tunnelling Microscopy Experiments and Density Functional Theory Simulations. *RSC Adv.* **2016**, *6*, 15071−15079.

(2) Romaner, L.; Heimel, G.; Brédas, J.-L.; Gerlach, A.; Schreiber, F.; Johnson, R. L.; Zegenhagen, J.; Duhm, S.; Koch, N.; Zojer, E. Impact of Bidirectional Charge Transfer and Molecular Distortions on the Electronic Structure of a Metal-Organic Interface. *Phys. Rev. Lett.* **2007**, *99*, 256801.

(3) Tseng, T.-C.; Urban, C.; Wang, Y.; Otero, R.; Tait, S. L.; Alcamí, M.; Écija, D.; Trelka, M.; Gallego, J. M.; Lin, N.; Konuma, M.; Starke, U.; Nefedov, A.; Langner, A.; Wöll, C.; Herranz, M. Á.; Martín, F.; Martín, N.; Kern, K.; Miranda, R. Charge-Transfer-Induced Structural Rearrangements at Both Sides of Organic/Metal Interfaces. *Nat. Chem.* **2010**, *2*, 374−379.

(4) Barja, S.; Stradi, D.; Borca, B.; Garnica, M.; Díaz, C.; Rodriguez-García, J. M.; Alcamí, M.; de Parga, A. L. V.; Martín, F.; Miranda, R. Ordered Arrays of Metal-Organic Magnets at Surfaces. *J. Phys.: Condens. Matter* **2013**, *25*, 484007.

(5) Martínez, J. I.; Abad, E.; Flores, F.; Ortega, J. Simulating the Organic-Molecule/Metal Interface TCNQ/Au(111). *Phys. Status Solidi B* **2011**, *248*, 2044−2049.

(6) Faraggi, M. N.; Jiang, N.; Gonzalez-Lakunza, N.; Langner, A.; Stepanow, S.; Kern, K.; Arnau, A. Bonding and Charge Transfer in Metal-Organic Coordination Networks on Au(111) with Strong Acceptor Molecules. *J. Phys. Chem. C* **2012**, *116*, 24558−24565.

(7) Della Pia, A.; Riello, M.; Stassen, D.; Jones, T. S.; Bonifazi, D.; De Vita, A.; Costantini, G. Two-Dimensional Core-Shell Donor-Acceptor Assemblies at Metal-Organic Interfaces Promoted by Surface-Mediated Charge Transfer. *Nanoscale* **2016**, *8*, 19004−19013.

(8) Blowey, P. J.; Velari, S.; Rochford, L. A.; Duncan, D. A.; Warr, D. A.; Lee, T.-L.; De Vita, A.; Costantini, G.; Woodruff, D. P. Re-Evaluating How Charge Transfer Modifies the Conformation of Adsorbed Molecules. *Nanoscale* **2018**, *10*, 14984−14992.

(9) Kadoya, T.; De Caro, D.; Jacob, K.; Faulmann, C.; Valade, L.; Mori, T. Charge Injection from Organic Charge-Transfer Salts to Organic Semiconductors. *J. Mater. Chem.* **2011**, *21*, 18421−18424.

(10) Koch, N.; Duhm, S.; Rabe, J. P.; Vollmer, A.; Johnson, R. L. Optimized Hole Injection with Strong Electron Acceptors at Organic-Metal Interfaces. *Phys. Rev. Lett.* **2005**, *95*, 237601.

(11) Earmme, T.; Jenekhe, S. A. Solution-Processed, Alkali Metal-Salt-Doped, Electron-Transport Layers for High-Performance Phosphorescent Organic Light-Emitting Diodes. *Adv. Funct. Mater.* **2012**, *22*, 5126−5136.

(12) Bin, Z.; Duan, L.; Qui, Y. Air Stable Organic Salt as an *n*-Type Dopant for Efficient and Stable Organic Light-Emitting Diodes. *ACS Appl. Mater. Interfaces* **2015**, *7*, 6444−6450.

(13) Lee, J.-H.; Kim, H.-M.; Kim, K.-B.; Kim, J.-J. Origin of Charge Generation Efficiency of Metal Oxide *p*-Dopants in Organic Semiconductors. *Org. Electron.* **2011**, *12*, 950−954.

(14) Floris, A.; Comisso, A.; De Vita, A. Fine-Tuning the Electrostatic Properties of an Alkali-Linked Organic Adlayer on a Metal Substrate. *ACS Nano* **2013**, *7*, 8059−8065.

(15) Woodruff, D. P. Surface Structure Determination Using X-Ray Standing Waves. *Rep. Prog. Phys.* **2005**, *68*, 743−798.

(16) Blowey, P. J.; Rochford, L. A.; Duncan, D. A.; Warr, D. A.; Lee, T.-L.; Woodruff, D. P.; Costantini, G. $_{p}$robing the Interplay Between Geometric and Electronic Structure in a Two-Dimensional K−TCNQ Charge Transfer Network. *Faraday Discuss.* **2017**, *204*, 97−110.

(17) Schlickum, U.; Decker, R.; Klappenberger, F.; Zoppellaro, G.; Klyatskaya, S.; Ruben, M.; Silanes, I.; Arnau, A.; Kern, K.; Brune, H.; Barth, J. V. Metal-Organic Honeycomb Nanomeshes with Tunable Cavity Size. *Nano Lett.* **2007**, *7*, 3813−3817.

(18) Geng, Y.; Li, P.; Li, J.; Zhang, X.; Zeng, Q.; Wang, C. STM Probing the Supramolecular Coordination Chemistry on Solid Surface: Structure, Dynamic, and Reactivity. *Coord. Chem. Rev.* **2017**, *337*, 145−177.

(19) Wang, Y.; Fabris, S.; White, T. W.; Pagliuca, F.; Moras, P.; Papagno, M.; Topwal, D.; Sheverdyaeva, P.; Carbone, C.; Lingenfelder, M.; Classen, T.; Kern, K.; Costantini, G. Varying Molecular Interactions by Coverage in Supramolecular Surface Chemistry. *Chem. Commun.* **2012**, *48*, 534−536.

(20) Tersoff, J.; Hamann, D. R. Theory of the Scanning Tunneling Microscope. *Phys. Rev. B: Condens. Matter Mater. Phys.* **1985**, *31*, 805−813.

(21) Zwick, C.; Baby, A.; Gruenewald, M.; Verwüster, E.; Hofmann, O. T.; Forker, R.; Fratesi, G.; Brivio, G. P.; Zojer, E.; Fritz, T. Complex Stoichiometry-Dependent Reordering of 3,4,9,10-Pertylenetatracarboxylic Dianhydride on Ag(111) upon K Intercalation. *ACS Nano* **2016**, *10*, 2365.

(22) Hermann, K. E.; Van Hove, M. A. *LEEDpat4*, version 4.2; Fritz Haber Institute: Berlin, 2015.

(23) Haags, A.; Rochford, L.A.; Felter, J.; Blowey, P.J.; Duncan, D.A.; Woodruff, D.P.; Kumpf, C. Growth and Evolution of TCNQ and K Coadsorption Phases on Ag(111). *New J. Phys.* **2020**, DOI: 10.1088/1367-2630/ab825f.

(24) Grimme, S. Semiempirical GGA-Type Density Functional Constructed with Long-Range Dispersion Correction. *J. Comput. Chem.* **2006**, *27*, 1787−1799.

(25) Gould, T.; Lebègue, S.; Ángyán, J.; Bučko, T. A Fractionally Ionic Approach to Polarizability and van der Waals Many-Body Dispersion Calculations. *J. Chem. Theory Comput.* **2016**, *12*, 5920−5930.

(26) Bučko, T.; Lebègue, S.; Ángyán, J.; Hafner, J. Extending the Applicability of the Tkatchenko-Scheffler Dispersion Correction *via* Iterative Hirshfeld Partitioning. *J. Chem. Phys.* **2014**, *141*, 034114.

(27) Tkatchenko, A.; Scheffler, M. Accurate Molecular van der Waals Interactions from Ground-State Electron Density and Free-Atom Reference Data. *Phys. Rev. Lett.* **2009**, *102*, 073005.

(28) Hirshfeld, F. L. Bonded-Atom Fragments for Describing Molecular Charge-Densities. *Theor. Chim. Acta* **1977**, *44*, 129−138.

(29) Bultinck, P.; Ayers, P. W.; Carbó-Dorca, R. Critical Analysis and Extension of the Hirshfeld Atoms in Molecules. *J. Chem. Phys.* **2007**, *126*, 144111.

(30) Baby, A.; Gruenewald, M.; Zwick, C.; Otto, F.; Forker, R.; Van Straaten, G.; Franke, M.; Stadtmüller, B.; Kumpf, C.; Brivio, G. P.; Fratesi, G.; Fritz, T.; Zojer, E. Fully Atomistic Understanding of the Electronic and Optical Properties of a Prototypical Doped Charge-Transfer Interface. *ACS Nano* **2017**, *11*, 10495−10508.

(31) Maurer, R. J.; Ruiz, V. G.; Camarillo-Cisneros, J.; Liu, W.; Ferri, N.; Reuter, K.; Tkatchenko, A. Adsorption Structures and Energetics of Molecules on Metal Surfaces: Bridging Experiment and Theory. *Prog. Surf. Sci.* **2016**, *91*, 72−100.

(32) Maurer, R. J.; Freysoldt, C.; Reilly, A. M.; Brandenburg, J. G.; Hofmann, O. T.; Björkman, T.; Lebègue, S.; Tkatchenko, A. Advances in Density-Functional Calculations for Materials Modelling. *Annu. Rev. Mater. Res.* **2019**, *49*, 1−30.

https://dx.doi.org/10.1021/acsnano.0c03133
ACS Nano 2020, 14, 7475−7483

(33) Succi, M.; Canino, R.; Ferrario, B. Atomic Absorption Evaporation Flow Rate Measurements of Alkali Metal Dispensers. *Vacuum* **1985**, *35*, 579−582.
(34) Neaton, J. B.; Hybertsen, M. S.; Louie, S. G. Renormalization of Molecular Electronic Levels at Metal-Molecule Interfaces. *Phys. Rev. Lett.* **2006**, *97*, 216405.
(35) Lüssem, B.; Riede, M.; Leo, K. Doping of Organic Semiconductors. *Phys. Status Solidi A* **2013**, *210*, 9−43.
(36) Lee, T.-L.; Duncan, D. A. A Two-Color Beamline for Electron Spectroscopies at Diamond Light Source. *Synch. Rad. News* **2018**, *31*, 16−22.
(37) Fisher, C. J.; Ithin, R.; Jones, R. G.; Jackson, G. J.; Woodruff, D. P.; Cowie, B. C. C. Non-Dipole Photoemission Effects in X-Ray Standing Wavefield Determination of Surface Structure. *J. Phys.: Condens. Matter* **1998**, *10*, L623−L629.
(38) Trzhaskovskaya, M. B.; Nefedov, V. I.; Yarzhemsky, V. G. Photoelectron Angular Distribution Parameters for Elements Z = 1 to Z-54 in the Photoelectron Energy Range 100−5000 eV. *At. Data Nucl. Data Tables* **2001**, *77*, 97−159.
(39) Blum, V.; Gehrke, R.; Hanke, F.; Havu, P.; Havu, V.; Ren, X.; Reuter, K.; Scheffler, M. *An Initio* Molecular Simulations with Numeric Atom-Centered Orbitals. *Comput. Phys. Commun.* **2009**, *180*, 2175−2196.
(40) Perdew, J. P.; Burke, K.; Ernzerhof, M. Generalised Gradient Approximation Made Simple. *Phys. Rev. Lett.* **1996**, *77*, 3865−3868.
(41) Ruiz, V. G.; Liu, W.; Zojer, E.; Scheffler, M.; Tkatchenko, A. Density-Functional Theory with Screened van der Waals Interactions for the Modelling of Hybrid Inorganic-Organic Systems. *Phys. Rev. Lett.* **2012**, *108*, 146103.
(42) Tkatchenko, A.; DiStasio, R. A.; Car, R.; Scheffler, M. Accurate and Efficient Method for Many-Body van der Waals Interactions. *Phys. Rev. Lett.* **2012**, *108*, 236402.
(43) DiStasio, R. A., Jr.; Gobre, V. V.; Tkatchenko, A. Many-Body van der Waals Interactions in Molecules and Condensed Matter. *J. Phys.: Condens. Matter* **2014**, *26*, 213202.
(44) Gould, T.; Bučko, T. C-6 Coefficients and Dipole Polarizabilities for All Atoms and Many Ions in Rows 1−6 of the Periodic Table. *J. Chem. Theory Comput.* **2016**, *12*, 3603−3613.
(45) Monkhorst, H. J.; Pack, J. D. Special Points for Brillouin-Zone Integrations. *Phys. Rev. B* **1976**, *13*, 5188−5192.
(46) Nečas, D.; Klapetek, P. Gwyddion: an Open-Source Software for SPM Data Analysis. *Cent. Eur. J. Phys.* **2012**, *10*, 181−188.
(47) Hjorth Larsen, A.; Mortensen, J. J.; Blomqvist, J.; Castelli, I. E.; Christensen, R.; Dułak, M.; Friis, J.; Groves, M. N.; Hammer, B.; Hargus, C.; Hermes, E. D.; Jennings, P. C.; Jensen, P. B.; Kermode, J.; Kitchin, J. R.; Kolsbjerg, E. L.; Kubal, J.; Kaasbjerg, K.; Lysgaard, S.; Maronsson, J. N.; et al. The Atomic Simulation Environment − A Python Library for Working with Atoms. *J. Phys.: Condens. Matter* **2017**, *29*, 273002.
(48) Nocedal, Jorge.; Wright, S. J. *Numerical Optimization*, 2nd ed.; Springer Science + Business Media: New York, 2006; pp 136−144.
(49) Sohail, B. *NOMAD repository*, DOI: 10.17172/NOMAD/2020.02.11-1 (accessed 2020-05-06).

https://dx.doi.org/10.1021/acsnano.0c03133
ACS Nano 2020, 14, 7475−7483